JOURNAL OF MATERIALS SCIENCE 28 (1993) 4925–4933

Effect of copper (II) content and metal vanadate formation on the structure, grain morphology and electrical conductance behaviour of $Mg_{1.0-x}$–Cu_x–$V_{2.0}$ ($0.0 \leq X \leq 1.0$) mixed oxide systems

M. M. GIRGIS
Chemistry Department, Catalysis Lab 514, Faculty of Science, Assiut University, Assiut, Egypt

A series of $Mg_{1.0-x}$–Cu_x–$V_{2.0}$ oxides as well as the corresponding metal vanadates ($0.0 \leq x \leq 1.0$) were prepared by calcination at temperatures between 500 and 1000 °C. X-ray diffraction and infrared spectral studies were used to identify the different phases present. Scanning electron microscopic investigations showed that the grain morphology not only depends on the sample calcination temperature, T_c, but also on its composition, x. The electrical conductance properties of the samples were studied between 100 and 350 °C. The variation of the conductance/and the activation energy values with x or T_c is discussed in terms of the oxides or vanadate semiconducting properties. A conduction mechanism involving hopping of electrons or polarons through M^n/M^{n-1} lattice sites is proposed.

1. Introduction

Several attempts [1–3] have been made to correlate the catalytic activity of some metal vanadates and/or the corresponding oxide mixtures with their semiconducting properties, in order to obtain a better understanding of the operation mechanism of these catalyst systems. Many of these complex systems have also drawn the attention of the solid state chemists [4, 5] and physicists [6, 7] due to their interesting structural [4, 5] electrical [7–10] and other physical properties [6, 7, 11]. One of the interesting systems is the $Mg_{1.0-x}$–Cu_x–$V_{2.0}$ oxide ($0.0 \leq x \leq 1.0$) series which is structurally controlled by the action of calcination temperature [5, 12]. The interest comes, also, from the fact that the individual parent oxides do not exhibit much electronic conductivity. It was reported that stoichiometric V_2O_5 [13] and CuO [14] are excellent electrical insulators, whereas the conductivity of MgO ($10^{-17}\Omega^{-1}cm^{-1}$ at 377 °C) is one of the lowest values ever reported for any material [14]. The $Mg_{1.0-x}$–Cu_x–$V_{2.0}$ mixed oxide systems calcined in the temperature range 500–1000 °C show drastic changes in structure, grain morphology and electrical conductivity either with increasing copper (II) content or calcination temperature. Therefore, and in connection with our previous studies on some related systems [2, 12, 15–17], the present study was undertaken to investigate the structural properties and semiconducting nature of the $Mg_{1.0-x}$–Cu_x–$V_{2.0}$ oxide system ($x = 0.0$) calcined in the temperature range 500–1000 °C. Our investigation was extended to study the effect of the progressive increase in copper (II) content ($0.1 \leq x \leq 1.0$) as well as the formation of metal vanadates on the structural and electrical conductance properties of these materials. Structural investigations were conducted by combining the results of X-ray diffraction, infrared spectroscopy, and scanning electron microscopy. To our knowledge no similar studies on our systems or other related ones are cited in the literature.

2. Experimental procedure

2.1. Materials

All the reagents used in the present investigation were of analytical grade (BDH chemicals). A series of $Mg_{1.0-x}$–Cu_x–$V_{2.0}$ mixed oxides (where $x = 0.0$, 0.1, 0.3, 0.5, 0.7, 0.9 and 1.0) were prepared by mixing ammonium metavanadate (AMV), with MgO and/or CuO. The mixing of AMV with the metal oxides was carried out in an agate mortar in the ratio of 2:1 [5, 14, 16]. In order to obtain a homogeneous mixture, a mixing time of 20 min was required. The parent mixtures were calcined in air for 5 h at 500, 700 and 1000 °C. The solids (500 °C samples) were slightly crushed to break up the crumbs, whereas the melts (700 and 1000 °C samples) were ground into fine powders after cooling.

2.2. Apparatus and techniques

The X-ray diffraction (XRD) patterns of the calcined samples were recorded using a Philips diffractometer (Model PW 1710) in the range of 2θ between 5° and

0022–2461

70°. A Philips generator operated at 40 kV and 30 mA, provided a source of CuK_α radiation (nickel filtered). The scanning speed was 2° min^{-1}. The diffraction patterns were matched with ASTM cards [18].

The infrared measurements were carried out in the range 4000–200 cm^{-1} using a Perkin Elmer infrared spectrophotometer (Model 599 B). The KBr disc technique was used where 2 mg fine substance was mixed with ~ 100 mg spectroscopically pure dry KBr powder by shaking for approximately 10 min in a vibrator. The mixture was then pressed in a special die under vacuum at $\sim 4 \times 10^3$ kg cm^{-2} using a hydraulic press.

The scanning electron microscope (SEM) investigations were performed on a Jeol JSM-T 200 scanning microscope (Jeol, Tokyo, Japan). The samples were prepared by sprinkling the powder lightly on to a double-sided adhesive tape which was mounted on an SEM specimen stub. The edge of the double-sided tape was printed with silver paint to minimize charging. Finally, the sample was sputter-coated with gold. Micrographs were obtained in a secondary electron imaging mode using a potential difference of 25 kV. SEM observations were carried out at a magnification of 350–10 000.

The electrical conductivity measurements were carried out using a conductivity cell described by Chapman *et al.* [19]. The temperature was controlled with a Digi-Sense temperature controller (Cole–Parmer Instrument Company, Chicago). The resistance measurements were made at 100–350 °C in air using a 610 C Solid-State Electrometer (Keithley Instruments). The reproducibility was within ± 2.0%.

3. Results and Discussion

3.1. X-ray diffraction and infrared spectral studies

The XRD patterns of $Mg_{1.0}$–$V_{2.0}$, $Mg_{0.5}$–$Cu_{0.5}$–$V_{2.0}$ and $Cu_{1.0}$–$V_{2.0}$ mixed oxide systems (i.e. of the samples with $x = 0.0$, 0.5 and 1.0, respectively) calcined at 500, 700 and 1000 °C for 5 h are represented in Fig. 1. The patterns for the composition of $x = 0.0$ show the diffraction lines of the primary oxides as major phases at 500 °C and indicate that magnesium metavanadate

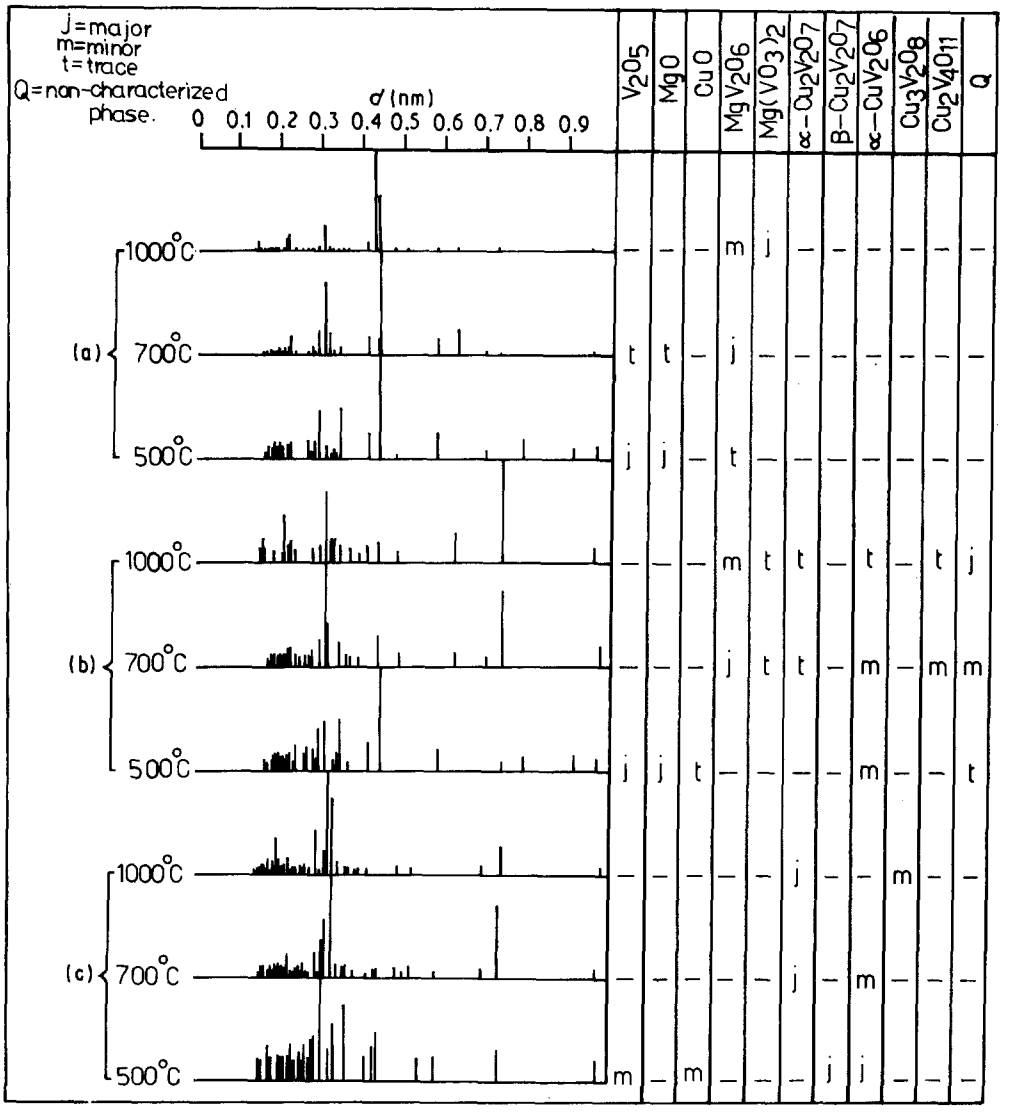

Figure 1 XRD for $Mg_{1.0-x}$–Cu_x–$V_{2.0}$ oxide systems: x = (a) 0.0, (b) 0.5, and (c) 1.0.

[11] becomes a major phase at 700 °C and predominates at 1000 °C [16]. The XRD patterns for the composition of $x = 1.0$ indicate that copper meta- and pyrovanadates are the major phases present at 500 °C, whereas copper pyrovanadate is the major one present at $T_c \geq 700$ °C. The XRD patterns also show that the major phases present in the $x = 0.5$ samples calcined at 500 °C are the primary metal oxides, whereas at $T_c \geq 700$ °C magnesium and copper vanadates (700 °C) and mixed metal vanadates (1000 °C) represent the major constituents [16].

The infrared spectra, in the region 500–1100 cm^{-1}, of $Mg_{1.0-x}$–Cu_x–$V_{2.0}$ mixed oxide ($x = 0.0$, 0.5 and 1.0) systems calcined at 500, 700 and 1000 °C and that of V_2O_5 calcined at 500 °C, for comparison, are shown in Fig. 2. Inspection of these spectra showed that V_2O_5 exhibits a band at 1000 cm^{-1} which is assignable to the V–O stretching vibration [20]. It also showed a combination band of V–O–V stretching and lattice vibration at 805 cm^{-1} [20, 21]. For the $Mg_{1.0-x}$–Cu_x–$V_{2.0}$ oxide samples calcined at 500 and 700 °C, these absorption bands were significantly weakened, especially for the 700 °C samples, whereas for the 1000 °C ones, these characteristic bands were not observed (for the composition of $x = 0.0$ and 1.0) or shifted to a higher frequency (the V–O absorption for the $x = 0.5$ sample). Hanuza *et al.* [22] reported the spectrum for MgV_2O_6. This spectrum shows absorption bands in the region 500–600 cm^{-1}. The presence of absorption in this region in our $x = 0.0$ samples calcined at 700 and 1000 °C supports the presence of magnesium metavanadate [11]. Spectra for the $x = 1.0$ samples calcined at 700 and 1000 °C possessed two absorptions at 960 and 810 cm^{-1} which can be assigned to V–O stretching characteristics of pyrovanadates [6]. The spectrum of the 1000 °C sample also possessed an absorption in the 840–860 cm^{-1} region, two others at 695 and 730 cm^{-1}, and a shoulder at 920 cm^{-1}. This structure also supports the existence of copper orthovanadate in our 1000 °C sample [23]. The two absorptions around 700 cm^{-1} may reflect the presence of different degrees of distortion of the orthovanadate structure [23]. The ν_3 antisymmetric stretch of $(VO_4)^{3-}$ anions [24] appears at 840–860 cm^{-1}, whereas the ν symmetric stretch appears as the shoulder at 920 cm^{-1} [25].

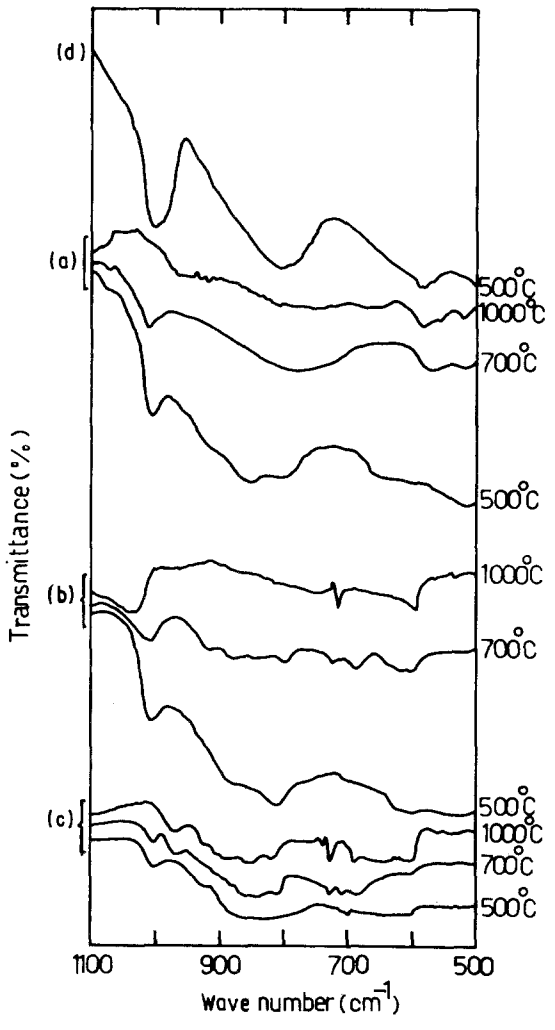

Figure 2 Infrared absorption spectra of $Mg_{1.0-x}$–Cu_x–$V_{2.0}$ oxide systems: x = (a) 0.0, (b) 0.5, and (c) 1.0, (d) V_2O_5.

3.2. Grain morphology examination

The results of the scanning electron microscopic investigation are shown in Figs 3–5. It is seen that the morphology of the particles not only depended on the sample calcination temperature, T_c, but also on its composition x. Fig. 3a and b show that $Mg_{1.0}$–$V_{2.0}$ oxide sample calcined at 500 °C containing agglomerates of less uniform size and shape, Fig. 3a. An examination of one of these agglomerates, Fig. 3b, showed that they consist of both rod-shaped particles and plate-like grains (of V_2O_5, as described elsewhere [25]). The pictures of the 700 °C sample, Fig. 3c, d show that it consisted of poorly defined particles, Fig. 3c, as well as many porous ones, Fig. 3d, whereas the picture of the 1000 °C sample, Fig. 3e, indicates that the grains are elongated bars of nearly rectangular section. This suggests that the external surface of the grains consists mainly of two practically perpendicular crystallographic planes. Kozlowski and Stadnicka [26] found that monocrystals of such vanadate solid solutions grown from the melt are of thin-plate shape with a large face corresponding to the (2 0 1) crystallographic plane, which supports our result.

Fig. 4 depicts the morphology of $Cu_{1.0}$–$V_{2.0}$ oxide system calcined at 500, 700 and 1000 °C. Close examination of a particle in the 500 °C sample indicated its spongy and porous nature, Fig. 4a and b. The grains of the powder sample of the 700 °C solid solution are mainly of elongated bar shape, Fig. 4c. Focusing the examination on one particle showed that the large faces have some surface roughness, Fig. 4d. In this respect, the picture of the 1000 °C sample shows a resemblance to that obtained for the 700 °C sample, Fig. 4e.

Electron micrographs of the $Mg_{0.5}$–$Cu_{0.5}$–$V_{2.0}$ oxide system calcined at 500, 700 and 1000 °C are shown in Fig. 5a–f. This figure shows clearly that the change of the grain morphology, characterizing these samples, with the calcination temperature was somewhat similar to that of the $x = 1.0$ ones.

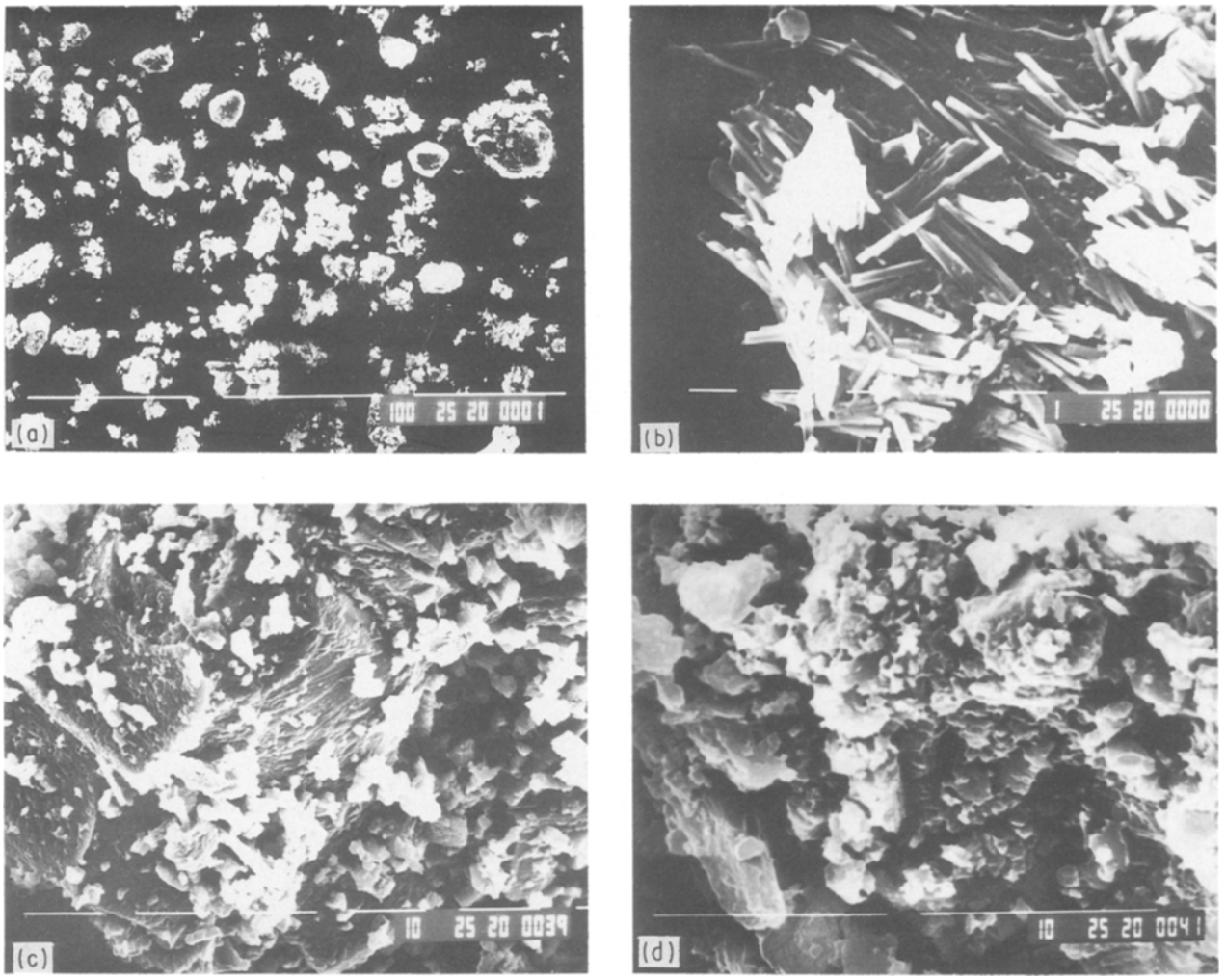

Figure 3 Scanning electron micrographs of $Mg_{1.0}$–$V_{2.0}$ oxide system calcined at different temperatures for 5 h. $T_c = 500\,°C$: (a) × 350, (b) × 10 000. $T_c = 700\,°C$: (c) × 1500, (d) × 5000. $T_c = 1000\,°C$: (e) × 5000.

3.3. Electrical conductivity measurements

Fig. 6 shows the temperature dependence of the electrical conductivity, σ, as a function of composition, x, for the $Mg_{1.0-x}$–Cu_x–$V_{2.0}$ oxide ($0.0 \leq x \leq 1.0$) systems calcined at 500, 700 and 1000 °C (a–c, respectively). Log σ values have been plotted against the reciprocal absolute temperature for all the compositions, x. The linear relationship obtained shows that the conductivity, σ, at a given temperature, T, can be expressed by the equation [27]

$$\sigma = \sigma_0 \exp(-E_\sigma/KT) \quad (1)$$

where σ_0 is a constant, E_σ the activation energy for conduction, K the Boltzmann constant, and T the absolute temperature. Accordingly, the slope of these lines was considered to give the activation energy for conduction. Values of E_σ obtained by least squares fitting of the data are plotted as a function of composition, x, in Fig. 7.

Examining the conductivity data represented in Fig. 6a for the 500 °C samples starting from the $Mg_{1.0}$–$V_{2.0}$ oxide system (i.e. at $x = 0.0$), one can distinguish a sharp conductivity increase with increasing concentration of copper ion content until $x = 0.3$, then it begins to fall at $x = 0.5$. A further increase of x increases the conductivity values up to $x = 0.9$, then they decrease slightly at $x = 1.0$. A comparison between the conductivity values of the 500 °C samples (Fig. 6a) with the activation energy of the various compositions (Fig. 7a) provides the observations: (i) variation of the activation energy values, E_σ, obeys the same order of conductivity, σ, change; (ii) among the different values of x, two compositions, namely $x = 0.3$ and 0.9, represent two inversion points in the activation energy pattern; (iii) the $x = 0.0$ composition

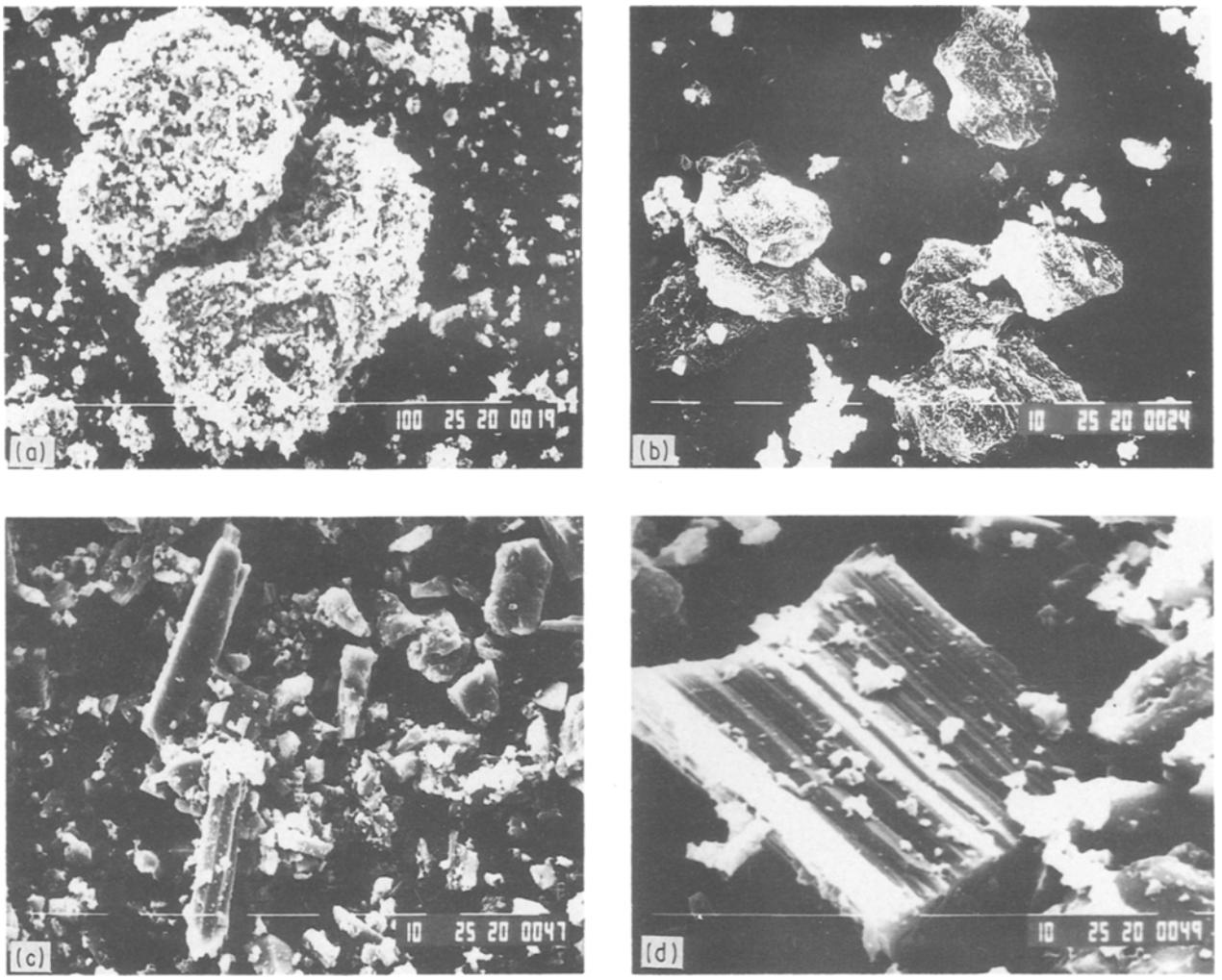

Figure 4 Scanning electron micrographs of $Cu_{1.0}$–$V_{2.0}$ oxide system calcined at different temperatures for 5 h. T_c = 500 °C: (a) × 500, (b) × 1000. T_c = 700 °C: (c) × 1500, (d) × 5000. T_c = 1000 °C: (e) × 500.

possesses the highest E_σ value, whereas the 0.3 composition possesses the lowest one. Inspection of the conductivity data of the 700 and 1000 °C samples (Fig. 6b and c) starting from the $x = 0.0$ composition, one can observe a pronounced conductivity increase with increasing concentration of Cu^{2+} ions until $x = 0.5$, then it decreases at $x = 0.7$. A further increase of x increases the conductivity values up to $x = 0.9$, then they decrease again at $x = 1.0$. A comparison between the electrical conductivity values of the 700 and 1000 °C samples (Fig. 6b and c) with the activation energy of the various compositions (Fig. 7b and c, respectively) showed that: (i) variation of the activation energy values, E_σ, obeys the same order of conductivity, σ, change, except for the composition of $x = 0.9$; (ii) there is a definite composition, i.e. $x = 0.5$, which represents an inversion point in the activation energy pattern; (iii) the $x = 0.0$ composition possesses the highest E_σ value, whereas the $x = 0.5$ composition possesses the lowest one. Generally, Fig. 6 indicates that: (i) the electrical conductance of the 700 °C samples is higher than that of the corresponding 500 °C ones, especially for the $x = 0.0$ and 0.5 compositions, with the exception of the samples with higher x-values, namely with $x = 0.9$ and 1.0, where they show slightly lower conductivity values; (ii) the conductance of the 1000 °C samples is slightly lower than that of the corresponding 700 °C ones, with the exception of the samples with lower x-values i.e. with $x = 0.0$ and 0.1, where they show slightly higher conductivity values. A comparative study of the effect of the calcination temperature, T_c, on the conduction activation energy of the $Mg_{1.0-x}$–Cu_x–$V_{2.0}$ oxide systems calcined at 500–1000 °C shows a strong dependence of E_σ on T_c. The noticeable trend is that E_σ decreases with increasing T_c in the order 500 °C > 700 °C > 1000 °C, Fig. 7.

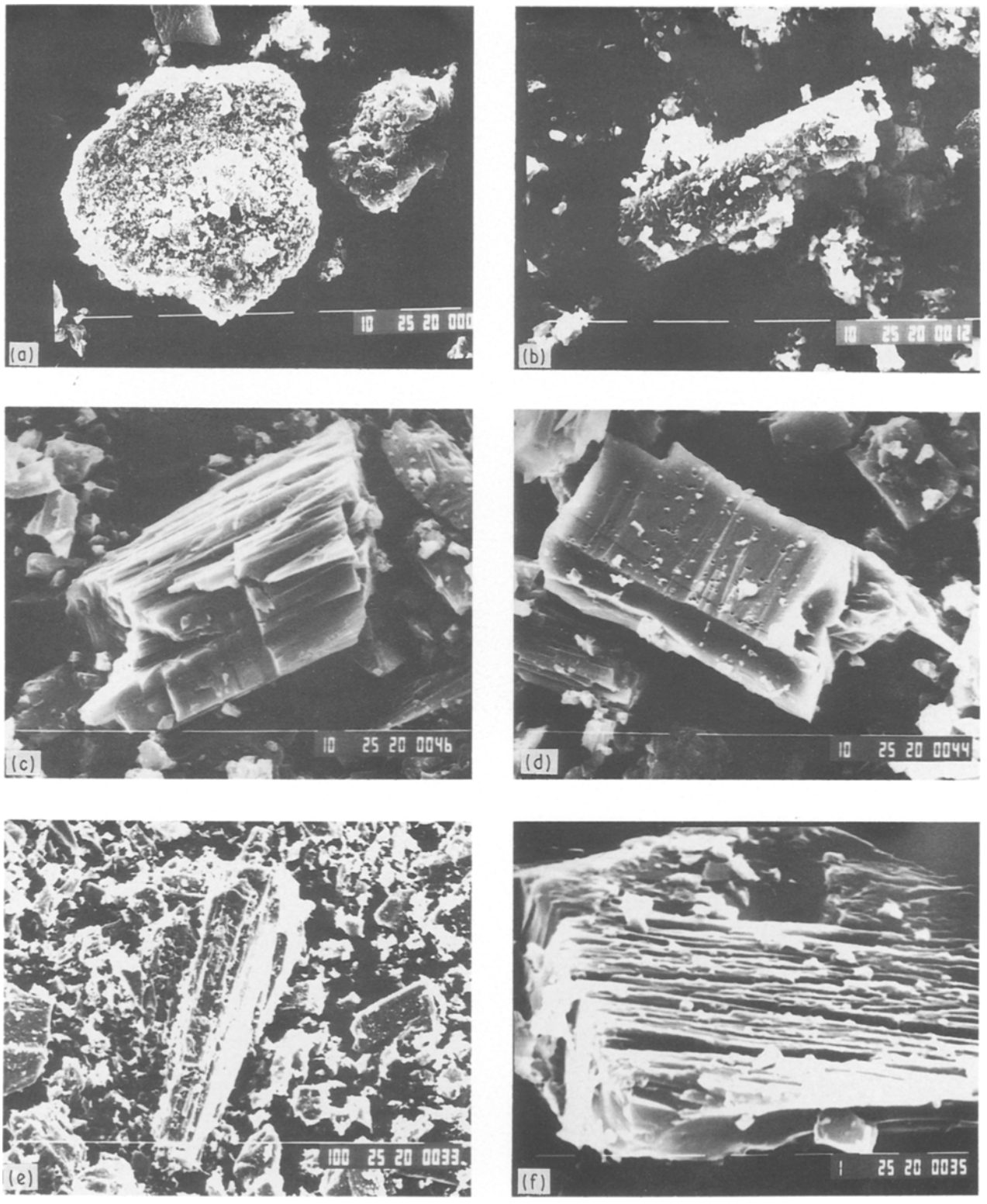

Figure 5 Scanning electron micrographs of $Mg_{0.5}$–$Cu_{0.5}$–$V_{2.0}$ oxide system calcined at different temperatures for 5 h. T_c = 500 °C: (a) × 1500, (b) × 2000. T_c = 700 °C: (c) × 3500, (d) × 3500. T_c = 1000 °C: (e) × 500, (f) × 10 000.

In order to explain the above conductivity data, one has to consider the probable conduction mechanisms in such materials. For the 500 °C samples, the composition with $x = 0.0$ represents the primary metal oxides. The conductivity of MgO in the temperature range studied was one of the lowest values ever reported in the literature [14] for any material, whereas that of pure V_2O_5 is zero [13, 28]. Thus, the conductivity of this composition must be expected to be low. The observed conductivity of the $x = 0.0$ sample can be attributed to the interaction between MgO and V_2O_5 according to Reaction 2, which leads to the enhancement [29] of the conduction electrons via hole production

$$3\,O + 2MgO = 2Mg|V|''' + V_2O_5 + 6|e|^{\cdot} \quad (2)$$

where $Mg|V|'''$ is the Mg^{2+} ion replacing the V^{5+} ion in its normal lattice site, and $|e|^{\cdot}$ is a defect electron produced.

The increase in σ with increasing x up to the

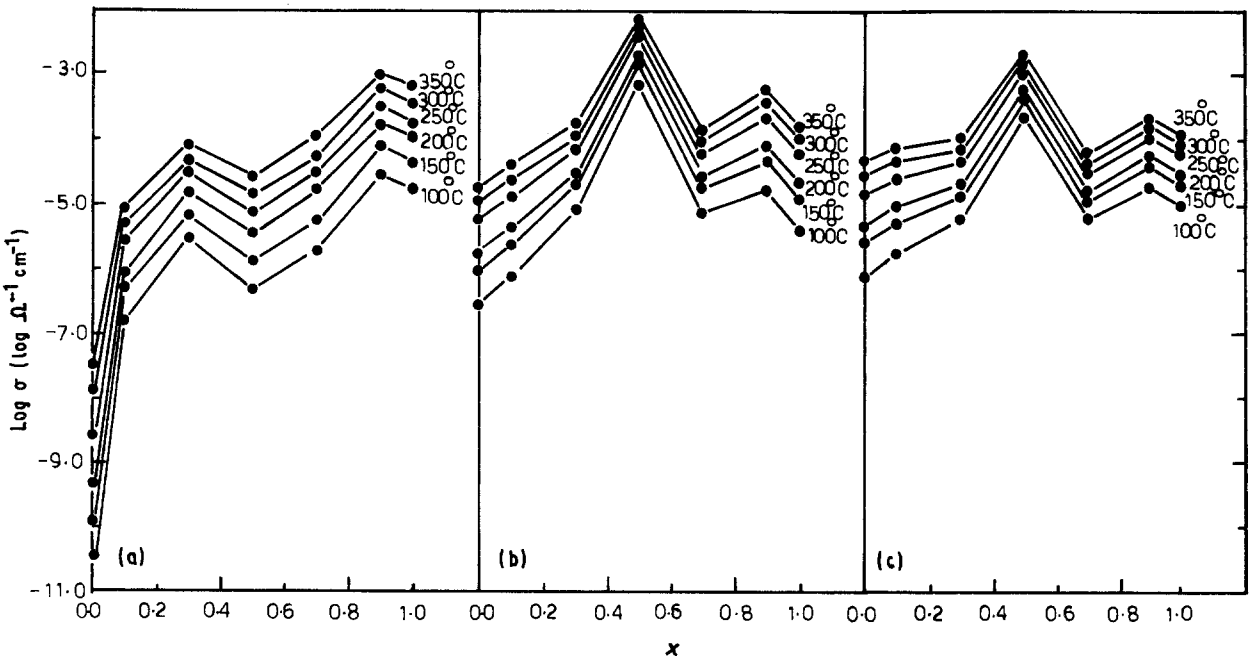

Figure 6 Variation of electrical conductivity, σ, values with x measured in the temperature range 100–350 °C for $Mg_{1.0-x}$–Cu_x–$V_{2.0}$ oxide systems calcined at (a) 500 °C (b) 700 °C and (c) 1000 °C.

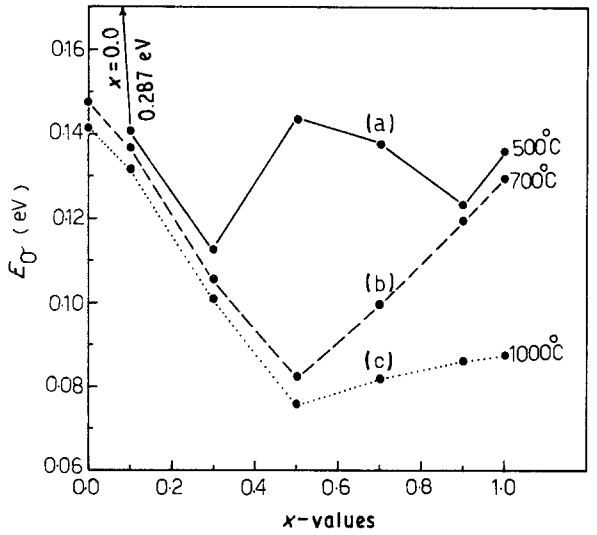

Figure 7 Variation of the activation energy, E_σ values with x for $Mg_{1.0-x}$–Cu_x–$V_{2.0}$ oxide systems calcined at (a) 500 °C, (b) 700 °C and (c) 1000 °C.

composition of $x = 0.3$ could be due to the progressive enhancement of the conduction electrons via more hole production by Reaction 3

$$3O + 2CuO = 2\ Cu|V|''' + V_2O_5 + 6|e|^{\cdot} \quad (3)$$

Furthermore, the lattice oxygen deficiency [29] of V_2O_5, accompanying Reactions 2 and 3, will give rise to some V^{4+} ions [30] so as to maintain electrical neutrality. The hopping of electrons between the adjacent V^{4+}/V^{5+} [1, 13, 31] ions increases the number of charge carriers which are responsible for the observed increase of σ. The sequence of E_σ values shows a Fermi potential of higher activation energy for $x = 0.0$, and of lower ones when the copper content, x, is increased to $x = 0.3$. At a composition of $x = 0.5$, the solid solution effect [29] was observed, which decreased the conductivity of the sample. The increase in conductivity at $x > 0.5$ can be attributed to the formation of the copper vanadates, Fig. 1. The conduction of such transition metal (t.m.) compounds was reported [32] to be characterized by a narrow 3 *d*-band [33] near the Fermi level. The presence of oxygen ions as a constituent in the lattice means that the 2*s* and 2*p*-oxygen orbitals strongly overlap the 4*s*- and 4*p*-orbitals of the 3*d* t.m. ions. This gives rise to a strong hybridization leading to a wide energy band gap between the top of the filled 2*p* band and the bottom of the 4*s* and 4*p* conduction bands. The narrow 3*d* bands of the t.m. cations in the studied series lie within this energy gap and are split by the crystal and exchange fields [2]. Thus, it can be said that two competing conduction processes exist; conduction by hopping of charge carriers in the narrow 3*d* band and normal band-like conduction in the 2*p* band, these two mechanisms dominating at lower and higher temperature, respectively. It is evident, from the small values of E_σ (≤ 0.144 eV) obtained for the activation energy of the different 500 °C samples at $x \geq 0.5$, that the hopping mechanism [32, 33] is the one operating in the employed temperature range. Consequently, the charge carriers are considered to be localized at the ions or vacant sites and the conduction occurs via a hopping-type process, which implies a thermally activated electronic mobility [34]. Because the activation energy in this case is often associated with the mobility of charge carriers rather than their concentration [35], one can consider that the composition $x = 0.5$ (characterized by the highest E_σ value at $x \geq 0.5$) represents the composition at which the charge carriers are more localized, due to a lower probability of at least two copper ions to be in adjacent positions, taking into consideration that no hopping-type conduction can take place between magnesium cations [14]. This concept allows us to infer that

the lowering of E_σ values characterizing the compositions $x = 0.7$ and 0.9 may be ascribed to the decrease of the isolated nature of the copper cations. In addition, according to Matkovich and Corbett [36] and Hibino *et al.* [37], the oxygen deficiency accompanying the solid-state formation of the vanadates at $x = 0.7$ and 0.9, i.e. the oxygen non-stoichiometry, will give rise to some V^{4+} ions in order to maintain the electrical neutrality. The hopping of electrons between the adjacent vanadium and/or copper sites, according to Reactions 4–6

$$V^{4+}/V^{5+} \rightleftharpoons V^{5+}/V^{4+} \quad [31] \qquad (4)$$

$$V^{4+}/Cu^{2+} \rightleftharpoons V^{5+}/Cu^{+} \quad [38] \qquad (5)$$

$$Cu^{+}/Cu^{2+} \rightleftharpoons Cu^{2+}/Cu^{+} \quad [16] \qquad (6)$$

increases the total number of charge carriers and accordingly the electrical conductivity of these samples. Although an increase in copper pair concentration must be expected with further deviation from the composition of $x = 0.5$, and consequently leads to an E_σ decrease, the composition at $x = 1.0$ behaves in the opposite manner. This can be referred to a significant role of the spin of the hopping electrons in the transfer process especially at higher concentration of copper ion pairs [39].

The samples prepared at 700 and 1000 °C are produced by quenching the melts to room temperature. The loss of oxygen from the melts and the change in their grain morphology cause a pronounced change in their conductance behaviour. Fig. 6a and b show that the conductivity of the 700 °C samples is higher than that of the corresponding 500 °C ones. In these samples, the low-valency vanadium and copper ions are produced due to loss of oxygen from the melt [33, 40]. The electrical conduction in these non-stoichiometric vanadates occurs mostly through the hopping of polarons [33, 34, 39, 41, 42], which consists of a *d*-electron and its polarized region in the lattice. The polarons generally move by hopping from one polarization well to the next one [2]. Fig. 8 illustrates the mechanism; Fig. 8a represents a small polaron with an electron localized in its potential well at equilibrium. If the electron is to be transferred, thermal fluctuations must ensure that the energies of the adjacent wells are

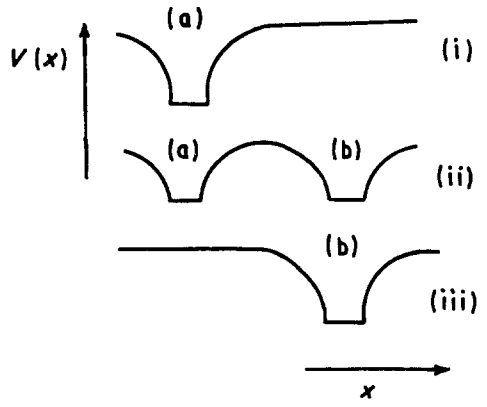

Figure 8 Potential wells on a pair of ions a and b during the hopping process: (i) before hopping; (ii) thermally activated state when electrons can move, and (iii) after hopping.

equal, as in Fig. 8b. It was established that the smallest activation energy which can produce this situation is when both wells have half the original depth [39], i.e. when the distribution of the t.m. cations allows at least two cations of the same metal to be in adjacent positions. As reported [7, 41–43], the conductivity of such vanadates depends on the ratio $\beta = [V^{4+}]/[V^{total}]$. It increases with the increasing β and is a maximum for a particular value of this ratio. In the system studied here, enhanced chemical reduction of V^{5+} ions might be achieved by interaction with the reduced ions of the added t.m., i.e. Cu^{+}, according to a chemical exchange mechanism of the form

$$Cu^{+} + V^{5+} \rightarrow Cu^{2+} + V^{4+} \qquad (7)$$

Thus, by increasing the copper content, x, of the 700 °C samples from $x = 0.0$ to $x = 0.5$ an oxidation–reduction mechanism as in Reaction 7, could easily be taking place with the increase of V^{4+} ions which increased the concentration ratio $[V^{4+}]/[V^{total}]$ and hence the conductivity increases. On increasing the sample copper (II) content, namely at $x > 0.5$, the concentration of V^{4+} ions decreases [44] according to the chemical exchange mechanism (Reaction 5 [38]) between two valency states of the two different transition elements. The reduction of V^{4+} ion concentration reduces the concentration ratio β and hence the conductivity decreases, Fig. 6b. Therefore, the decrease in conductivity at $x > 0.5$ may, in our case, be ascribed to pairing of mixed ions in the form of oxygen–bridged associates [39]. Thus, the effect of the copper ion is expected to alter the ratio of concentrations of reduced valency vanadium ions to the concentration of normal valency vanadium ions, and thus to control the transition probabilities of conduction electrons and hence the electrical conductivity. It appears that there exists a critical concentration of copper content (i.e. at $x = 0.5$) for which β and hence the electrical conductivity showed a maximum. In the light of the above discussion the change in the activation energy for hopping conduction could be ascribed to the copper (II) content which alters the reduced valency ratio, β, in the vanadates under investigation.

The variation of the electrical conductance of the 1000 °C samples with Cu^{2+} content, x, has a trend similar to that obtained for the 700 °C samples, Fig. 6b, c. Under the same experimental conditions of both composition ($0.3 \leq x \leq 1.0$) and temperature, comparative studies relating the conductance behaviour for the 700 and 1000 °C samples reveal that the concentration ratio $[V^{4+}]/[V^{total}]$ decreases with increasing calcination temperature, T_c, from 700 °C to 1000 °C.

The decrease of the activation energy, E_σ, with the increase of the sample calcination temperature in the order 500 °C > 700 °C > 1000 °C (Fig. 7) can be attributed to the increase in the mobility of the electrons through the hopping process, because E_σ in this case is associated with the mobility of charge carriers rather than their concentration. Electron micrographs of the systems investigated (Figs 3–5) show that the particle size increases and the porosity decreases on increasing

T_c from 500 °C up to 1000 °C. This permits a higher mobility of charge carriers, and accordingly lower E_σ values, with increasing T_c.

References

1. D. K. CHAKRABARTY, D. GUHA, I. K. BHATNAGAR and A. B. BISWAS, *J. Catal.* **45** (1976) 305.
2. R. M. GABR, A. M. EL-AWAD and M. M. GIRGIS, *J. Mater. Chem. Phys.* **30** (1991) 69.
3. D. J. COLE, C. F. CULLIS and D. J. HUCKNALL, *J. Chem. Soc. Farad. Trans. 1* **72** (1976) 2744.
4. K. MOCALA and J. ZIOLKOWSKI, J. Solid State Chem. **69** (1987) 299.
5. *Idem, ibid.* **71** (1987) 552, and papers quoted therein.
6. P. K. SINHAMAHAPATRA and S. K. BHATTACHARYYA, *J. Thermal Anal.* **9** (1976) 279.
7. M. A. HASSAN, M. N. KHAN and C. A. HOGARTH, *Phys. Status Solidi (a)* **105** (1988) 609.
8. J. H. PERLSTEIN and M. J. SIENKO, *J. Chem. Phys.* **44** (1968) 174.
9. B. G. GOLOVKIN, A. A. FOTIEV and A. A. NEUIMIN, *Zh. Fiz. Khim.* **45** (1971) 2247.
10. M. V. VOLZHENSKII, M. V. PASHKOVSKII and L. C. SEVEKOLKINA, *Russ. J. Inorg. Chem.* **8** (1963) 129.
11. R. C. KERBY and J. R. WILSON, *Can. J. Chem.* **51** (1973) 1032.
12. R. M. GABR, A. M. EL-AWAD and M. M. GIRGIS, *Thermal Anal.* **37** (1991) 249.
13. O. G. PALANNA, *Indian J. Chem.* **17A** (1979) 442.
14. D. ADLER, in "Treatise on Solid State Chemistry", Vol. 2 "Defects in Solids", edited by N. B. HANNAY (Plenum Press, New York, London, 1975) pp. 283, 286, 292.
15. A. M. EL-AWAD, R. M. GABR and M. M. GIRGIS, *Thermochem. Acta* **184** (1991) 205.
16. M. M. GIRGIS, R. M. GABR and A. M. EL-AWAD, *Croat. Chim. Acta* **64** (1991).
17. R. M. GABR, M. M. GIRGIS and A. M. EL-AWAD, *Thermochem. Acta* (1991).
18. W. F. MCCLUNE (ed.), "Powder Diffraction File (Inorganic Phases)", (JCPDS International Centre for Diffraction Data, USA, 1984).
19. P. R. CHAPMAN, R. H. GRIFFITH and J. D. F. MARSH, *Proc. R. Soc. Lond.* **224** (1954) 419.
20. M. INOMATA, A. MIYAMOTTO and Y. MURAKAMI, *J. Catal.* **62** (1980) 140.
21. K. TARAMA, S. YOSHIDA, S. ISHIDA and H. KOKIOKA, *Bull. Chem. Soc. Jpn* **41** (1968) 2840.
22. J. HANUZA, B. JEZOWSKA-TRYEBRATOWSKA and W. OGANOWSKI, *J. Molec. Catal.* **29** (1985) 109.
23. M. A. CHAAR, D. PATEL, M. C. KUNG and H. H. KUNG, *J. Catal.* **105** (1987) 483.
24. W. P. GRIFFITH and F. GONZALES, *J. Chem. Soc. Dalton Trans.* (1972) 1416.
25. A. BAIKER and D. MONTI, *J. Catal.* **91** (1985) 361.
26. R. KOZLOWSKI and K. STADNICKA, *J. Solid State Chem.* **39** (1981) 271.
27. S. R. MORRISON, "Chemical Physics of Surface" (Plenum, New York, 1977) p. 70.
28. J. W. MELLOR, "A Comprehensive Treatise on Inorganic and Theoretical Chemistry", Vol. IX (Longmans, Green, London, New York, Toronto, 1957) p. 755.
29. K. M. ABD EL-SALAAM, E. A. HASSAN and A. A. SAID, *Surface Technol.* **21** (1984) 327.
30. V. MUCKA, *Collect. Czech. Chem. Commun.* **49** (1984) 1.
31. J. J. BARA, B. F. BOGACZ, M. PEKALA and A. A. POLACZEK, *J. Solid State Chem.* **28** (1985) 143.
32. R. B. YADAV, J. Phys. Chem. Solids **44** (1983) 697.
33. D. ADLER and J. FEINLEIB, *Phys. Rev.* **B2** (1970) 3112.
34. D. KUMAR, C. D. PARSAD and O. PARKASH, *J. Phys. Chem. Solids* **51** (1990) 73.
35. B. A. MULLA and V. S. DARSHANE, *Indian J. Chem.* **24 A** (1985) 359.
36. V. I. MATKOVICH and P. M. CORBETT, *J. Amer. Ceram. Soc.* **44** (1961) 128.
37. T. HIBINO, O. WATANABE and M. TARIDA, *Kogyo Kagaku Zasshi*, **68** (1965) 2322.
38. L. D. BOGOMOLOVA, T. F. DOLGOLENKO, V. N. LAZUKIN and N. V. PETROVYKH, *Sov. Phys. DOKl.* **18** (1973) 61.
39. P. POMONIS and J. C. VICKERMAN, *J. Catal.* **55** (1978) 88.
40. G. CANNERI, *Gaz. Chem. Ital.* **58** (1928) 6.
41. N. F. MOTT, *J. Non-Cryst. Solids* **1** (1968) 1.
42. I. G. AUSTIN and N. F. MOTT, *Adv. Phys.* **18** (1968) 41.
43. L. MURAWSKI, C. H. CHUNG and J. D. MACKENZIE, *J. Non-Cryst. Solids* **32** (1979) 91.
44. A. GHOSH and B. K. CHAUDHURI, *ibid.* **103** (1988) 83.

Received 2 December 1991
and accepted 24 March 1992